Available online at www.sciencedirect.com
ScienceDirect
Chemical Physics Letters 441 (2007) 294–299
CHEMICAL PHYSICS LETTERS
www.elsevier.com/locate/cplett

The effect of the morphology of nanocrystalline CeO_2 on ethanol reforming

Wei-In Hsiao, Ya-Shiuan Lin, Yu-Chie Chen *, Chi-Shen Lee *

Department of Applied Chemistry and Institute of Molecular Science, National Chiao Tung University, 1001 Ta-Hsueh Road, Hsinchu 30010, Taiwan

Received 16 February 2007; in final form 4 May 2007
Available online 10 May 2007

Abstract

CeO_2 nanocrystals of cubic and rod shape have been synthesized under hydrothermal conditions on controlling the pH, temperature and duration of reaction. High-resolution transmission electron microscopy indicates that exposed crystal planes are {110} and {100} for rods but {100} for cubes. These nanocrystals have been used in the preparation of a Rh/CeO_2 catalyst on an Al_2O_3 support to test the catalytic activity for ethanol reforming. These catalysts as prepared show good H_2 selectivity compared to catalysts with irregular CeO_2 nanoparticles. The {100}/{110}-dominant surface structures play a crucial role in enhancing ethanol reforming; this reaction is important for fuel-cell applications.

1. Introduction

Ceria (CeO_2) possesses many attractive properties that make it highly promising for diverse applications such as solid electrolytes or anode materials in solid oxide fuel cells [1–3], automotive three-way catalysts [4–6], a water-gas-shift catalyst [7], ultraviolet absorbers [8], oxygen sensors [9], and catalysts for dehydrogenation of higher alcohols [10,11]. Under particular experimental conditions CeO_2 nanocrystals with a specific shape and a narrow distribution of size can be prepared in high yield [12–16]. CeO_2 nanocrystals exhibit a behavior dependent on shape in some catalytic processes: for instance, the nanorods and nanocubes exhibit a greater capacity to store oxygen than nanoparticles [17]; the rate of oxidation of CO on CeO_2 nanorods is greater than on CeO_2 nanoparticles [18], and the rate of CO oxidation on gold supported on CeO_2 nanoparticles is a hundred times higher than that of Au on a regular CeO_2 support [19,20]. Theoretical calculations of both surface energy and catalytic activity indicate that the {100} and {110} faces are more active than the {111} surfaces [21–25], consistent with experimental findings. A means to increase the fraction of reactive {100} and {110} planes, and thus to decrease the fraction of less reactive {111} planes in CeO_2 nanoparticles, is important for a new generation of CeO_2-based catalysts. Among many catalysts, the Rh/CeO_2 catalyst exhibits excellent selectivity for hydrogen and excellent stability for the steam reforming of ethanol [10,26]. The catalytic properties of a Rh-ceria catalyst might be greatly influenced by the nature of the exposed surface. Although much work has been performed on the synthesis and catalytic activity of CeO_2 nanocrystals of various shapes [17–19,27], there is no report treating the effect of CeO_2 morphology on the catalytic effect in the reforming of ethanol. We report here the synthesis and characterization of CeO_2 nanoparticles and the effect of CeO_2 morphology on ethanol reforming.

2. Experiments

2.1. Synthesis and characterization of CeO_2 nanoparticles and catalyst

(1) CeO_2 nanocrystals of rod and cubic shape were synthesized under hydrothermal conditions [17,18]. In general, $Ce(NO_3)_3 \cdot 6H_2O$ (0.5 g, 99.9%, Alfa Aesar) was dissolved

* Corresponding authors. Fax: +886 3 5723764.
E-mail addresses: yuchie@mail.nctu.edu.tw (Y.-C. Chen), chishen@mail.nctu.edu.tw (C.-S. Lee).

0009-2614/$ - see front matter © 2007 Elsevier B.V. All rights reserved.
doi:10.1016/j.cplett.2007.05.024

in deionized water (10 mL) to produce a transparent solution, to which was added NaOH (99%, J.T. Baker) solution in a fixed amount with rigorous stirring for 10 min. The concentration of OH^- was controlled on adding deionized water. The solution contained some white precipitate, which was transferred to a Teflon-lined stainless-steel autoclave. The optimum conditions for the preparation of a nanorod sample were $[OH^-] = 15$ M, $T = 150$ °C, reaction duration 10 h, and then cooling to 23 °C. After that reaction, the solid products were filtered and rinsed with first deionized water and then methanol. The major products from the hydrothermal synthesis were $Ce(OH)_3$ rods of length 100–200 nm. The dried products were calcined at 300 °C to form CeO_2 nanorods. For a nanocube sample, the best conditions were reaction with concentrated NaOH ($[OH^-] = 15$ M) and heating at 150 °C for 48 h. After that reaction, the solid products were filtered and rinsed with first deionized water and then methanol. The major products from the hydrothermal synthesis were CeO_2 nanocubes with average size 40–50 nm. The nanoparticles of all CeO_2 products have a characteristic light yellow color. The crystallinity, purity, crystal morphology and size of CeO_2 products were analyzed with powder X-ray diffraction, transmission electron microscopy (TEM) and scanning electron microscopy (SEM) with energy-dispersive spectroscopy (EDS). All CeO_2 products were obtained as pure phases in a high yield.

(2) (a) A catalyst with CeO_2 nanorods/nanocubes was prepared on impregnating granulated alumina (Al_2O_3, 300 m^2/g, average diameter 1.2 mm) with an aqueous solution of $Rh(NO_3)_3 \cdot 2H_2O$ (0.0136 g, 99.9%, Alfa Aesar) and CeO_2 nanocrystals (0.2 g), followed by ultrasonic irradiation for 1 h, oven drying at 120 °C for 6 h and finally calcination at 500 °C for 1 h. (b) A catalyst with irregular CeO_2 particles was first prepared on impregnating alumina support (2.000 g) with a known amount of $Ce(NO_3)_3 \cdot 6H_2O$ (0.5 g), followed by oven drying at 60 °C for 6 h and finally calcination in air at 400 °C for 6 h. The resulting material was subsequently impregnated with $Rh(NO_3)_3 \cdot 2H_2O$ (0.0136 g) using the same conditions as 2a. The Rh content of all catalysts were 5% mass and the loading of each catalyst was ~0.20 g per 2 g of alumina support. EDS analyses on Rh/CeO_2 catalysts revealed all constituent elements.

(3) XRD data were collected on a powder diffractometer (Bruker D8, Cu Kα, 40 kV/40 mA). Semiquantitative microprobe analysis was performed with a scanning electron microscope (SEM, Hitachi S4700, Tokyo, Japan) equipped with an energy-dispersive spectroscopy (EDS) detector. Data were acquired with an accelerating voltage 15 kV. TEM images were obtained with a microscope (Philips TECNAI 20). Samples were generally prepared on depositing a drop of dilute nanoparticle solution in toluene onto carbon-coated Cu grids.

2.2. Apparatus and product analysis

Tests of catalytic performance were performed with an apparatus similar to that described elsewhere [28–32]. The system was equipped with mass-flow controllers for controlling the composition of the carrier gas and an HPLC pump for injecting the fed liquid (water/ethanol (3/1, mole ratio)). Reaction gases, supplied from high-pressure gas cylinders, had ultrahigh purity. Ethanol was analytic grade (Merck). The liquid was pumped to a steel chamber in which it was evaporated and in which it could be mixed (when desired) with an air stream from the mass-flow controllers. The gaseous mixture was fed to the reactor through silica tubing (inner diameter 4 mm, length ~15 cm). The temperature of the resulting gaseous mixture was maintained at 200 °C inside a furnace. The reactor was loaded with catalytic specimens of length up to 1.5 cm (~0.1 g), and having a silica glass-wool seal between the catalyst and the reactor walls. Two thermocouples were placed inside the vaporizer and on top of the catalyst to monitor the temperature profiles. A six-port valve (Valco) served to direct samples of the effluent to the injection port of a GC–MS system (Trace Ultra DSQ) equipped with a PLOT capillary column (30 m × 0.53 mm ID; Carboxen 1010, TCD detector, carrier gas = Ar, internal standard = N_2) to GC and a PLOT column (30 mm × ID 0.53 mm, Supel-Q, carrier gas = He) to a mass spectrometer. A condenser was placed before the latter column to condense and to remove H_2O, unreacted ethanol and other hydrocarbons from the gaseous stream.

The response factors of the TCD and MS detectors were determined by means of gaseous streams of known composition. The H_2 peak was integrated and compared against a calibration line produced from pure H_2 gas (>99.999% purity) before the experiments. The column oven was set at 45 °C and the TCD temperature was set at 200 °C. Argon or helium (>99.999% purity) served as carrier gas at a flow rate 72 mL/min with a split ratio 24. For the MS measurement, the mode of ionization was electron impact; data were collected in the full-scan mode. All experiments were performed at atmospheric pressure. In a typical experiment, after a fresh catalyst was placed in the reactor, the reactant stream with a water/ethanol molar ratio 3/1 was introduced into the reactor ($T = 200$ °C), in which it was heated, vaporized, and mixed with Ar carrier gas and air, and finally passed through the catalyst. The injection rate of ethanol was adjusted to control the C/O ratio. The temperature of the catalyst was increased rapidly to ~800 °C, and the product streams were fed into the GC–MS system. Freshly made catalysts were used to study the hydrogen selectivity at various C/O ratios. The overall reaction can be described as follows [10]

$$C_2H_5OH + 2H_2O + 1/2O_2 \rightarrow 2CO_2 + 5H_2$$

The catalytic activity was evaluated in terms of hydrogen selectivity (S_{H_2}), which is defined as the molar ratio of the product H_2 (5 mol expected from the above reactions per mol ethanol) to the hydrogen production per mole of ethanol (3 mol H_2/mol ethanol). Ethanol and other hydrocarbon products were condensed in water and analyzed with a mass spectrometer. In all cases the results showed that

most ethanol had reacted. For each catalyst, the reforming experiments were repeated several times and their results were reproducible.

3. Results and discussion

Powder XRD patterns for CeO_2 nanocrystals of rod and cubic shape are shown in Fig. 1. All diffraction peaks show broad lines and can be indexed to imply a purely cubic phase (space group: $Fm\bar{3}m$) with lattice parameters $a = 5.42(1)$ and $5.40(1)$ Å for rod and cubic samples, respectively, in satisfactory agreement with a literature value $a = 5.411$ (1) Å.

The SEM image of CeO_2 nanorods (Fig. 2a) shows an average diameter and a length in the ranges 20–30 and 100–200 nm, respectively. The inset of Fig. 2a presents a TEM image and a SAED pattern of a CeO_2 nanorod that reveals an interplanar d-spacing 0.28(1) nm attributed to (200) and (020) planes, indicating preferred growth in the direction [110]. This result and other TEM images indicate that the CeO_2 nanorods are enclosed with {110} and {100} planes, consistent with a previous report on the synthesis of CeO_2 nanorod [18]. The CeO_2 nanocubes as obtained had a regular cubic shape with a mean length 40 nm (Fig. 2b). A TEM lattice image taken from a single CeO_2 cube clearly shows interplanar d-spacings 0.27(1) nm, which is near that of (002) planes of cubic CeO_2 (inset of Fig. 2b). This result indicates that the CeO_2 cubes were enclosed with {100} planes.

With GC–MS we investigated the effect of CeO_2 morphology on H_2 selectivity (S_{H_2}) in ethanol reforming; the setup is according to the literature. [10,29] Three catalysts using CeO_2 nanorods (**1**), nanocubes (**2**) and irregular particles (**3**) were prepared. The effect of the C/O ratio on the catalytic performance of Rh/CeO_2 catalysts **1**–**3** (5% mass)

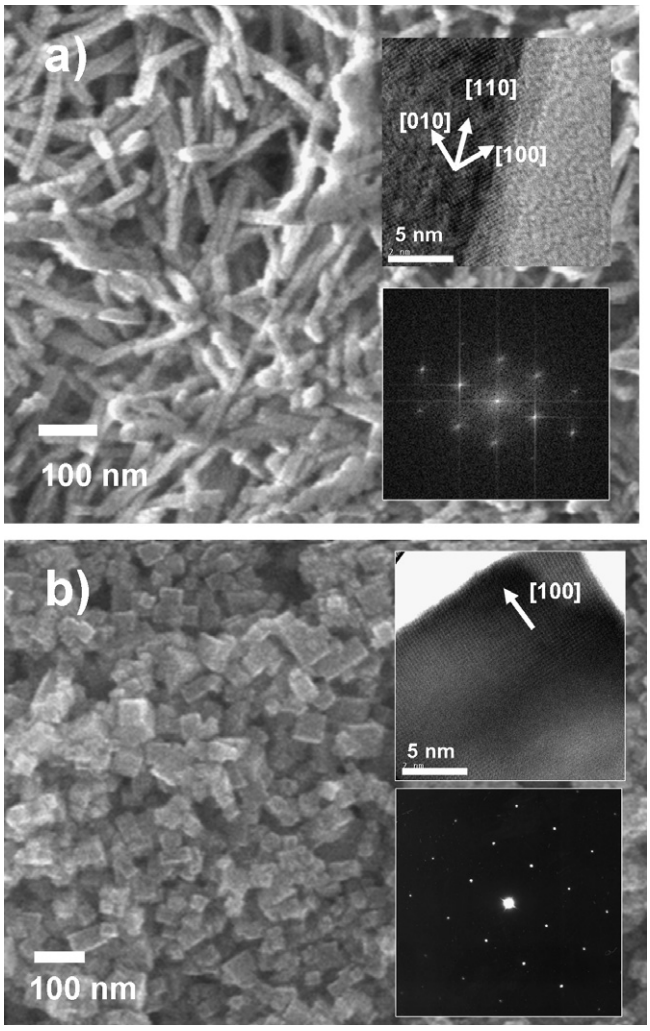

Fig. 2. SEM images of CeO_2 nanorods (a) and nanocubes (b). The insets are TEM images and SAED patterns for a single rod and cubic sample, respectively.

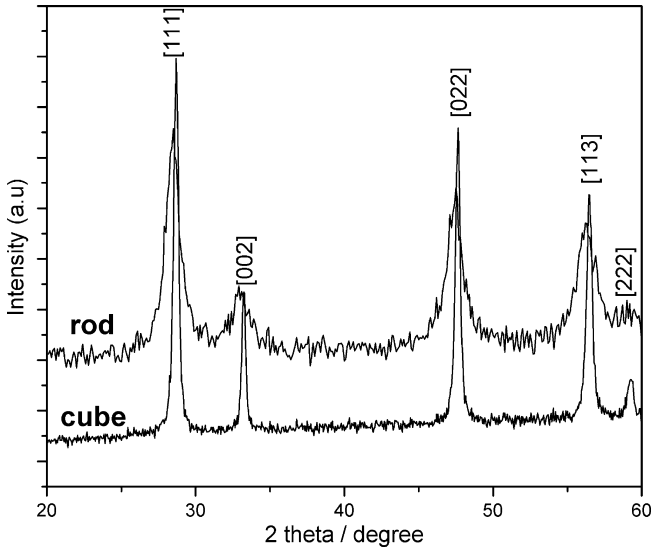

Fig. 1. Powder XRD patterns for CeO_2 nanocrystals of rod and cubic shapes.

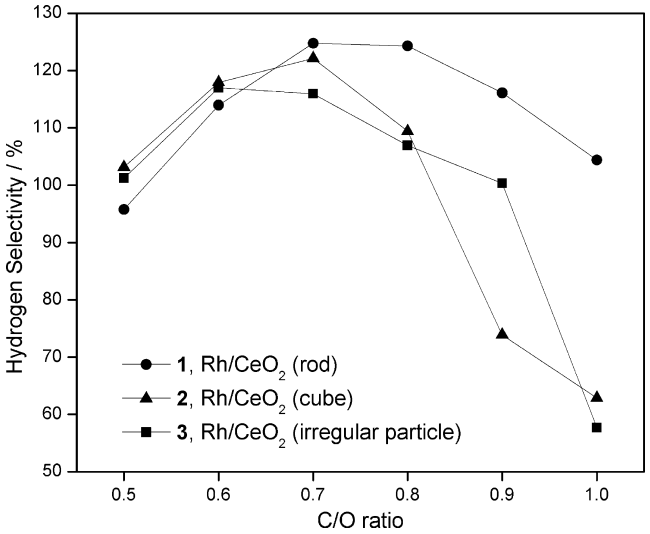

Fig. 3. Hydrogen selectivity as a function of C/O ratio obtained over Rh/CeO_2 catalysts **1**–**3**.

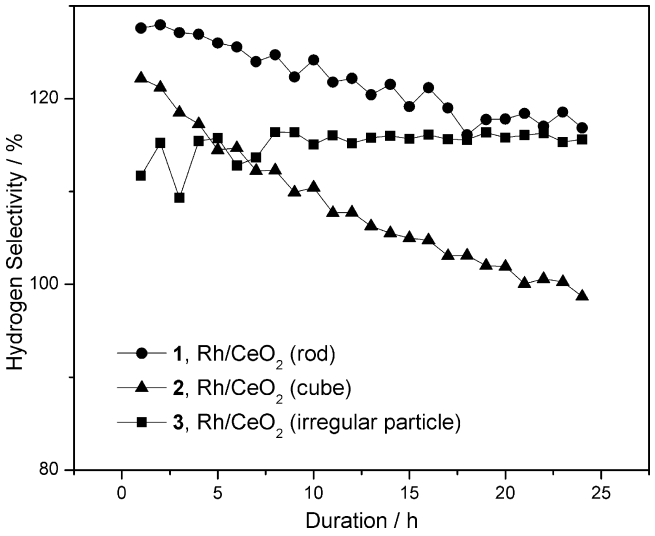

Fig. 4. Hydrogen selectivity as a function of duration on stream obtained over Rh/CeO_2 catalysts **1**–**3**.

is shown in Fig. 3 with the C/O ratio varied from 0.5 to 1.0. The results indicate that, for catalysts **1** and **2**, S_{H_2} increased gradually on increasing C/O to attain maximum values 126% and 122% at C/O = 0.7, respectively, which are larger than the maximum S_{H_2} of catalyst **3** (S_{H_2} = 116% at C/O ratio ~0.6). The optimized S_{H_2} for catalyst **3** is consistent with the literature value. [10] S_{H_2} of **1** decreased from 126% to 100% upon altering the C/O ratio from 0.7 to 1.0, whereas S_{H_2} of **2** decreased sharply from 122% to 60%. The rate of conversion of ethanol is hence affected by the morphology of nanocrystalline CeO_2. The poor catalytic performance of **3** is attributed to an even distribution of {111}, {110}, {100} and other surfaces, which have a smaller concentration of {100} and {110} facets than for CeO_2 rods and cubes. The effect of CeO_2 morphology on the catalytic performance of Rh/CeO_2 catalysts might reflect the surface energy and concentration of active sites on CeO_2 nanocrystals. These results indicate that the surface activity of (100) ~ (110) is greater than for (111) planes of CeO_2 crystal.

The stability tests were performed with the optimized S_{H_2} for the C/O ratio of each catalyst; S_{H_2} is plotted as a function of duration on stream (Fig. 4). The results indicate that all catalysts suffered a small deactivation during 24 h on stream.

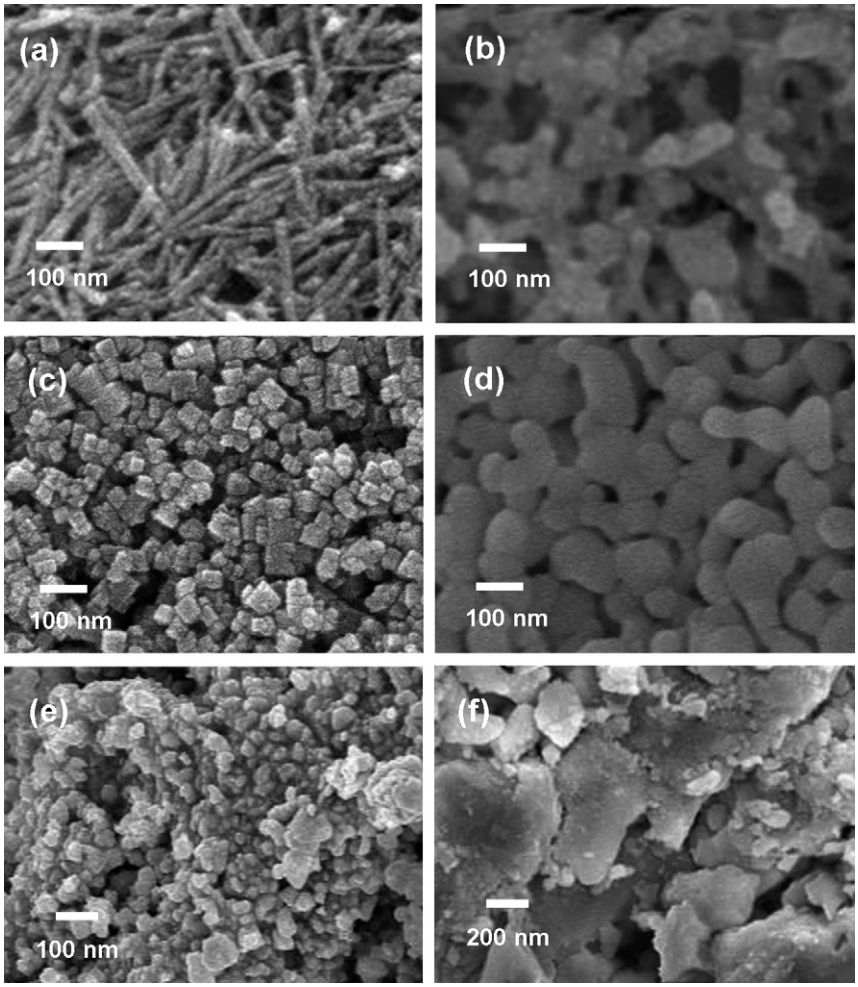

Fig. 5. SEM images of Rh/CeO_2 catalysts **1**–**3** before (a, c, and e) and after (b, d, and f) the ethanol-reforming reaction for 24 h.

For catalyst **1**, S_{H_2} varied insignificantly in decreasing slightly from the initial value 126–120% after 24 h on stream. In contrast, S_{H_2} of catalyst **2** altered significantly from the initial value 122% to 100% after 24 h on stream. S_{H_2} of **3**, similar to the literature value [10], was less sensitive to the duration of reaction and remained constant at 115(1)% during 24 h of reaction. These results indicate clearly that CeO_2 nanoparticles with a specifically exposed surface affect the overall catalytic activity under working conditions. Why the catalyst with cubic CeO_2 showed the least activity after 24 h of reaction is unclear; one reason might be that the particle size increased significantly, leading to a decreased surface area so that S_{H_2} alters accordingly. We confirmed this hypothesis with SEM measurements.

As the CeO_2 morphology is the key to ethanol reforming, we analyzed the shape of CeO_2 particles before and after 24 h of reforming; SEM images of catalysts **1**–**3** appear in Fig. 5. The morphology of each individual particle detected before and after ethanol reforming indicates a significant modification of the size and shape of the CeO_2 particle, as deduced from the SEM images. The common feature of catalysts **1** and **2** was the change of nanocrystal from clear-edge to smooth-edge particles. Before the reforming, the surface of Al_2O_3-supported catalysts was covered with CeO_2 nanorods (Fig. 5a) and nanocubes (Fig. 5b) of uniform shape. The morphology of CeO_2 nanocrystals after reforming reveals that the special exposure surfaces were lost, indicating that the reaction occurred primarily on the CeO_2 surfaces. In the case of rod nanoparticles, a distortion at the corners of the nanoparticle was observed. The SEM image shows that the nanocrystals of rod shape are distorted to form round corners after the reaction (Fig. 5b). For a catalyst with nanocubes of CeO_2, the cubical shape transformed to a spherical shape, the sides becoming rounded and the average size of particles increasing to ~80 nm (Fig. 5c and d). These CeO_2 particles became aggregated after reaction for 24 h. The rounding of the edges and corners of the rod and cubic nanoparticles might result from a rapid exchange of oxygen atoms in Ce^{+3}/Ce^{+4} reactions. The particle size of catalyst **3** was increased from ~50 nm to >100 nm after 24 h of ethanol reforming (Fig. 5e and f). These results show that exchange of oxygen with CeO_2 occurred during the experiment, which produced a subtle change from a clear-edge single crystal to nearly spherical particles of large size. After the shape of CeO_2 nanoparticles altered, S_{H_2} decreased accordingly. For a catalyst with more effective production of hydrogen, a more stable metal-oxide surface for reforming ethanol is necessary for fuel-cell applications.

4. Conclusion

Rh/CeO_2 catalysts with CeO_2 nanocrystals of rod and cubic shape exhibit satisfactory catalytic activity, and are thus good candidates for using in ethanol-reforming processors for fuel-cell applications. This shape-dependent property provides an efficient means to investigate other catalysts consisting of metal oxides of controlled size and shape. Both rod and cubic samples showed initially a rate of conversion of H_2 greater than for an irregular CeO_2 catalyst, but their activity gradually decreased because of an altered CeO_2 morphology. A possible way to maintain the stability of CeO_2 nanocrystals is to dope a stable metal, such as Ti or Zr; additional work in this direction is in progress.

Acknowledgements

Institute of Nuclear Energy Research, Atomic Energy Council, Taiwan (contract NL940251) and National Science Council (contracts NSC94-2113-M-009-012, 94-2120-M-009-014) supported this research.

References

[1] S.C. Singhal, K. Kendall, High-temperature Solid Oxide Fuel Cells: Fundamentals, Design and Applications, Elsevier, Oxford, New York, 2003.
[2] A. Trovarelli, Catalysis by Ceria and Related Materials, Imperial College Press, London, 2002.
[3] Y.M. Chiang, E.B. Lavik, I. Kosacki, H.L. Tuller, J.Y. Ying, J. Electroceram. 1 (1997) 7.
[4] W.J. Stark, J.D. Grunwaldt, M. Maciejewski, S.E. Pratsinis, A. Bai, Chem. Mater. 17 (2005) 3352.
[5] S.C. Laha, R. Ryoo, Chem. Commun. (2003) 2138.
[6] M. Lunderg, B. Skaerman, F. Cesar, L.R. Wallenberg, Micropor. Mesopor. Mater. 54 (2002) 97.
[7] Q. Fu, H. Saltsburg, M. Flytzani-Stephanopoulos, Science 301 (2003) 935.
[8] T. Masui, K. Fujiwara, K.I. Machida, G.Y. Adachi, Chem. Mater. 9 (1997) 2197.
[9] P. Jasinski, T. Suzuki, H.U. Anderson, Sensor Actuat. B 95 (2003) 73.
[10] G.A. Deluga, J.R. Salge, L.D. Schmidt, X.E. Verykios, Science 303 (2004) 993.
[11] L. Mo, X. Zheng, C.-T. Yeh, Chem. Phys. Chem. 6 (2005) 1470.
[12] Z.L. Wang, X. Feng, J. Phys. Chem. B 107 (2003) 13563.
[13] C. Ho, J.C. Yu, T. Kwong, A.C. Mak, S. Lai, Chem. Mater. 17 (2005) 4514.
[14] W.Q. Han, L. Wu, Y. Zhu, J. Am. Chem. Soc. 127 (2005) 12814.
[15] C. Tang, Y. Bando, B. Liu, D. Golberg, Adv. Mater. 17 (2005) 3005.
[16] A. Vantomme, Z.Y. Yuan, G. Du, B.L. Su, Langmuir 21 (2005) 1132.
[17] H.X. Mai, L.D. Sun, Y.W. Zhang, R. Si, W. Feng, H.P. Zhang, H.C. Liu, C.H. Yan, J. Phys. Chem. B 109 (2005) 24380.
[18] K. Zhou, X. Wang, X. Sun, Q. Peng, Y. Li, J. Catal. 229 (2005) 206.
[19] S. Carrettin, P. Concepción, A. Corma, J.M.L. Nieto, V.F. Puntes, Angew. Chem. Int. Edit. 43 (2004) 2538.
[20] J. Guzman, S. Carrettin, A. Corma, J. Am. Chem. Soc. 127 (2005) 3286.
[21] D.C. Sayle, S.A. Maicaneanu, G.W. Watson, J. Am. Chem. Soc. 124 (2002) 11429.
[22] Z.P. Liu, S.J. Jenkins, D.A. King, Phys. Rev. Lett. 94 (2005) 196102.
[23] Z. Yang, T.K. Woo, M. Baudin, K. Hermansson, J. Chem. Phys. 120 (2004) 7741.
[24] Y. Jianga, J.B. Adams, M.v. Schilfgaarde, J. Chem. Phys. 123 (2005) 064701.
[25] Z.-P. Liu, S.J. Jenkins, D.A. King, Phys. Rev. Lett. 94 (2005) 196102.
[26] S. Bernal, J.J. Calvino, M.A. Cauqui, J.M. Gatica, C. Larese, J.A.P. Omil, J.M. Pintado, Catal. Today 50 (1999) 175.
[27] P.X. Huang et al., J. Phys. Chem. B 109 (2005) 19169.

[28] L. Garcia, R. French, S. Czernik, E. Chornet, Appl. Catal. A 201 (2000) 225.
[29] D.K. Liguras, K. Goundani, X.E. Verykios, Int. J. Hydrogen Energy 29 (2004) 419.
[30] S. Cavallaro, Energ. Fuels 14 (2000) 1195.
[31] A.N. Fatsikostas, D.I. Kondarides, X.E. Verykios, Chem. Commun. (2001) 851.
[32] A.N. Fatsikostas, D.I. Kondarides, X.E. Verykios, Catal. Today 75 (2002) 145.